JOURNAL OF GUIDANCE, CONTROL, AND DYNAMICS
Vol. 16, No. 1, January-February 1993

Time-Variant Analysis of Rotorcraft Systems Dynamics—An Exploitation of Vector Processors

F. M. L. Amirouche,* M. Xie,† and N. H. Shareef†
University of Illinois at Chicago, Chicago, Illinois 60680

In this paper a generalized algorithmic procedure is presented for handling constraints in mechanical transmissions. The latter are treated as multibody systems of interconnected rigid/flexible bodies. The constraint Jacobian matrices are generated automatically and suitably updated in time, depending on the geometrical and kinematical constraint conditions describing the interconnection between shafts or gears. The type of constraints are classified based on the interconnection of the bodies by assuming that one or more points of contact exist between them. The effects due to elastic deformation of the flexible bodies are included by allowing each body element to undergo small deformations. The procedure is based on recursively formulated Kane's dynamical equations of motion and the finite element method, including the concept of geometrical stiffening effects. The method is implemented on an IBM-3090-600j vector processor with pipe-lining capabilities. A significant increase in the speed of execution is achieved by vectorizing the developed code in computationally intensive areas. An example consisting of two meshing disks rotating at high angular velocity is presented. Applications are intended for the study of the dynamic behavior of helicopter transmissions.

I. Introduction

MOST engineering devices are made up of assembled parts and many of these parts have mechanical interconnections or surface/line contacts between them. In most cases, it is important to know the contact conditions in order to predict accurately the strength, stresses, and other mechanical characteristics of such systems. A geared transmission/rotorcraft system is one such example.

The subject of rotor dynamics has been the interest of many researchers in the past decade.[1-6] The major focus of such research has been limited to the analysis of rotors. This includes the extraction of the natural frequencies and mode shapes making use of methods such as the transfer matrix and finite elements. The reliability of these rotorcraft systems is then closely related to the vibration characteristics of the rotor as a whole and its components in particular with the permissible level of vibrational stress.

Most prominent and critical among several components used in transmissions are gears and shafts. In these systems, the power and speed are transmitted through meshing gears. The contact between meshing gear teeth is of crucial importance. A thorough understanding of this phenomenon of contact between gear teeth will help in controlling the reliability and performance of transmission/rotorcraft systems.

In the past few years, research has been conducted in this area of contacting bodies, in particular, when the bodies are elastic. The finite element technique has been used extensively by a number of researchers to study the contact phenomenon, the reason being that the finite element method (FEM) is conceptually simple, easily adaptable to high-speed electronic computations, and applicable to a large class of geometries, materials, and loading conditions.

A numerical procedure developed for solving the two-dimensional elastic contact problems with friction is presented in Ref. 7. This is a generalization of the procedure presented by Fracauilla and Zienkiewicz.[8] This method uses the flexibility matrix obtained by inversion of the condensed stiffness matrix formed by eliminating all nodes, except those where contact is likely to take place and those with external forces.

The application of the mixed finite element method for two-dimensional elastic contact problems has been investigated by Tseng and Olson.[9] In this method the displacements and stresses are treated as variables. Some of these displacement variables are treated as natural boundary conditions in the contact region. An algorithmic procedure for dealing with numerical analysis of a highly nonlinear variational inequality encountered in the study of contact problems with nonclassical friction laws is described in Ref. 10. A special bond element is proposed for the solution of the contact problem by the finite element method in Ref. 11. A modified finite element method has been presented by Chan and Tuba for solving problems of elastic bodies in contact using three-node triangular elements.[12] Contact problems involving sticking frictional sliding and separation under large deformation for the analysis of planar and axisymmetric cases have been dealt with by Bathe and Chaudhary.[13] A new kind of finite element has been presented by Vijayakar et al. to work efficiently for bodies that are either prismatic or quasiprismatic in shape.[14] The frictional contact problem through the imposition of geometric constraints on the configuration at which compatibility conditions are violated is studied by using FEM.[15] Simo et al. has carried out the research in the area of numerical solutions of large deflection involving finite strains, subject to contact constraints, and unilateral boundary conditions and exhibiting constitutive responses.[16]

The solution to variational inequalities arising in contact problems of structural dynamics through a linear finite element approach is presented in Ref. 17. A similar study[18] used the finite element method to deal with surface nonlinearities in structural mechanics, with special emphasis on contact and fracture mechanics problems. In this paper an attempt has been made to develop a general method for the study of contact conditions in the multielastic body systems that undergo large rigid-body motion. Though the methodology presented is a general one, the study has been restricted to rotorcraft systems. These systems have gears and shafts as their important components. Gears are connected to the shafts through simple mechanisms like splines, whereas gears have contact conditions with the other mating gears through meshing gear teeth. This paper presents an algorithmic procedure to deal with such contact conditions. Constraint equations are generated for these contact conditions by assuming a point/line/surface con-

Received Feb. 20, 1991; revision received Nov. 12, 1991; accepted for publication April 29, 1992.

*Professor, Department of Mechanical Engineering.
†Ph.D. Research Assistant, Department of Mechanical Engineering.

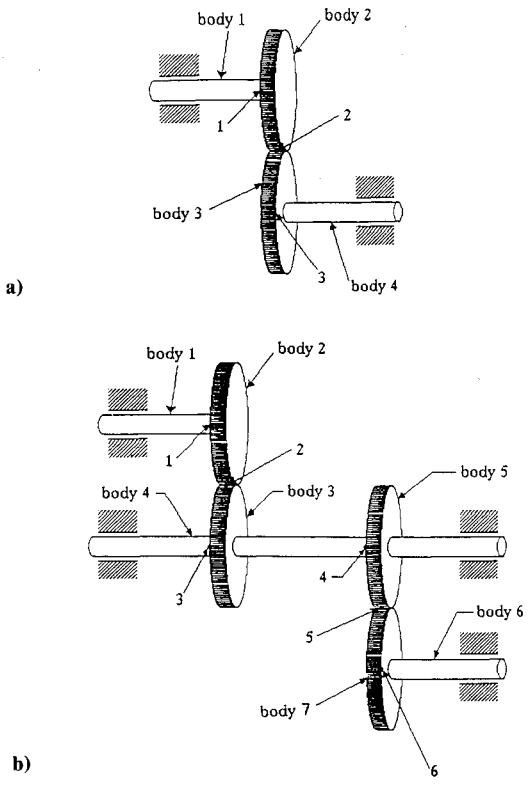

Fig. 1 Simple gear train.

tact between the bodies. The surfaces of the bodies having contact are discretized using three-dimensional brick elements. Based on the assumed point/line/surface contact between the bodies, one, two, or more pairs of nodal points will be in contact with each other.

The constraints are classified into two types: 1) a shaft and a gear, or 2) a gear and a gear. An algorithm for the automatic generation of the Jacobian matrices associated with those constraints is presented. The dynamical equations of motion given in this paper are based on the method developed in Ref. 19, which uses a recursive formulation of Kane's equations combined with the finite element method, concepts of strain energy, and the modal coordinate reduction technique. This includes the complete interaction between the rigid and flexible motions. The associated modes of vibration are selected a priori (preprocessor) and integrated in the equations through the single relationship between the nodal coordinates of the elements and the modal coordinates.

The procedure developed here has been implemented on various supercomputers (IBM 3090, CRAY). The computational efficiency in the execution of the code has been improved using indexed-reference arrays[20] and a proposed vectorization technique. An illustrative example is given where the contact conditions are simulated by discretizing two meshing disks rotating at high speed. The time-variant constraints are generated automatically and solved with the system equations of motion. The associated constraint forces at the contacting points are evaluated and plotted.

II. Concepts of Vector Processing

A supercomputer is generally characterized by three main features: 1) high computational speed; 2) large main memory; and 3) fast and large secondary memory. The high computational speed is of obvious desirability. A large main memory is useful in processing large data and operating large-scale programs from main memory. Secondary memory is important in many scientific jobs because the data simply cannot fit in main memory. In such cases, secondary storage may be regarded as an overflow of main memory.[22-24]

The aspect of high computational speed is achieved through the use of vector processors, which have the capability of handling vectors, arrays, and matrices more efficiently. These vector processors make use of the "pipe-lining" technique that allows overlapping of instructions. A vector instruction applies a single operation, such as a floating-point add, to a sequence of operands. In contrast, a scalar instruction applies a simple operation to a single operand (or operand pair). Therefore, speed is achieved by a kind of microparallelism, in which different stages of pipeline work simultaneously on different data. In general, performance increases with the vector length up to a limit that depends on the implementation of pipeline.

The pipeline can be used effectively only when data are supplied to it at a sufficiently high rate. How this may be achieved depends on architectural details that vary significantly from one computer to another. One is the memory-to-memory architecture, in which source operands and intermediate and final results are retrieved directly between the pipelines and main memory. CDC-Star-100 and Cyber-205 are examples of such systems.

Multivector processing further enhances the speeds of execution by subdividing the loop and distributing the work to various available processors. Based on the vectorizability of the code or vice versa, it is referred to as vector-concurrent or scalar-concurrent. In the case of a Do-loop nest for which the innermost loop is vectorizable, the next outer loop is subdivided and distributed to available processors. The code in this case is called concurrent-outer-vector-inner (COVI). The field of multi-elastic-body dynamics is a potential candidate for such applications. The method developed in this paper is implemented in a code called dynamics analysis of rotorcraft systems (DARS) and the pipe-lining feature of the vector processors has been exploited for the application presented.

III. Recursive Formulation of the Equations of Motion

The equations of motion of a flexible multibody system expressed in matrix form and based on Kane's equations are obtained from Ref. 21; they are expressed as follows:

$$\mathfrak{M}\dot{\mathcal{Y}} + \mathcal{P} + \mathcal{Q} + \lambda\mathcal{J} = \mathcal{F} \tag{1}$$

where $\mathfrak{M}$, $\mathcal{Q}$, λ, $\mathcal{J}$, $\mathcal{F}$, and $\mathcal{P}$ represent the coefficients' matrices associated with accelerations, the generalized speeds' quadratic velocity vector, the c-dimensional vector of undetermined multipliers, the constraint Jacobian matrix, generalized external forces, and stiffness due to the strain energy of the flexible bodies in the system, respectively. The details for the derivation of these matrices can be found in Ref. 21. The stiffness due to the strain energy is given by

$$\mathcal{P} = \begin{bmatrix} 0 \\ 0 \\ \chi^T[K+G]\chi\eta \end{bmatrix} \tag{2}$$

where K and G are the block diagonal matrices, whose diagonal submatrices are K^k and G^k, referring to the structural stiffness and geometric stiffness for body K. The χ is the shape matrix and η the modal coordinate.

Using the residual weights W_i, W_j, W_k corresponding to the Gauss points $(\mu_{gp}, \bar{\omega}_{gp}, \vartheta_{gp})$, we can write the equation for the element stiffness $\mathcal{K}^{ki}$ as

$$\mathcal{K}^{ki} = \sum_{i=1}^{\mu_{gp}} \sum_{j=1}^{\bar{\omega}_{gp}} \sum_{k=1}^{\vartheta_{gp}} \mathcal{B}^{kiT}(\mu,\bar{\omega},\vartheta) \cdot \mathcal{D}^{ki} \times \mathcal{B}^{ki}(\mu,\bar{\omega},\vartheta) \cdot \det\left[\mathcal{J}(\mu,\bar{\omega},\vartheta)\right] W_i \cdot W_j \cdot W_k \tag{3}$$

where $\mathcal{B}$, $\mathcal{D}$, and $\mathcal{J}$ are the strain-displacement matrix, stress-strain matrix, and Jacobian of the transformation from the

local x_1, x_2, x_3 coordinates (floating reference frame for the flexible body) to the dimensionless coordinates of the finite element $(\mu, \bar{\omega}, \vartheta)$.

The computation of $\mathcal{Z}^{ki}$ can be carried out numerically using

$$\frac{\partial \mathcal{U}^{ki}}{\partial \Delta^{ki}} = \mathcal{Z}^{ki}\Delta^{ki} \tag{4}$$

where $\mathcal{U}^{ki}$ and Δ^{ki} are the strain energy component and the vector of nodal elastic displacements for the ith element of body k, respectively. This can be written in terms of the components of the nonlinear strain displacements γ_{12}, γ_{23}, and γ_{31} by using the nonlinear theory of elasticity for linear elastic materials as

$$\mathcal{U}^{ki} = \frac{1}{2} G \sum_{i=1}^{\mu_{gp}} \sum_{j=1}^{\bar{\omega}_{gp}} \sum_{k=1}^{\vartheta_{gp}} (2\gamma_{xy}^{s})^2 + (2\gamma_{yz}^{s})^2 + (2\gamma_{zx}^{s})^2 \times \det\left[\mathcal{J}(\mu, \bar{\omega}, \vartheta)\right] W_i \cdot W_j \cdot W_k \tag{5}$$

where G is the modulus of rigidity for the material used. Further, the nonlinear strain displacement relation could be expressed in terms of the derivatives of the elastic deformations u_1, u_2, and u_3 along the x_1, x_2, and x_3 directions as

$$\gamma_{ab}^{s} = \frac{1}{2}\left(\frac{\partial u_a}{\partial x_b} + \frac{\partial u_b}{\partial x_a} + \sum_{c=1}^{3} \frac{\partial u_c}{\partial x_a} \cdot \frac{\partial u_c}{\partial x_b}\right), \quad a,b = 1,2,3 \tag{6}$$

The procedure for arriving at the global structural stiffness matrix and global geometric stiffness matrix at the body and system level follows from the standard finite element method.

IV. Derivation of the Constraint Equations

Use of partial velocity arrays in the recursive formulation of the dynamical equations of motion renders a noteworthy benefit, the automatic generation of the constraint equations. Basically, the various constraints could be broadly classified as 1) closed loops; 2) prescribed motions; and 3) contact between interconnected bodies.

Closed loops are a common type of constraint, found in various mechanisms. The joining point, where the closed loop occurs, can be reached in two ways from the fixed inertial reference frame. The constraint equations can be written based on the differentiation of the position vectors. The specification of the kinematical quantities such as speeds and angular velocities as a function of time form the second type of constraints. The constraint equations for this case could be written by equating the expression for the kinematical quantity to the function of time. Specified angular speed for a transmission system is one of the examples for such constraints. The details of the foregoing two types of constraints can be found in Ref. 19.

In a similar fashion, the third type of constraint mentioned here is defined by the number of points used to describe the contact between gear/shaft and gear/gear bodies. In fact, this is a special case of a closed-loop type of constraint with its extension to points and surfaces in contact. It will be shown in the following sections of the paper that the Jacobian matrices associated with the generalized coordinate derivatives can be generated automatically for the cases of both the rigid and flexible gears/shafts.

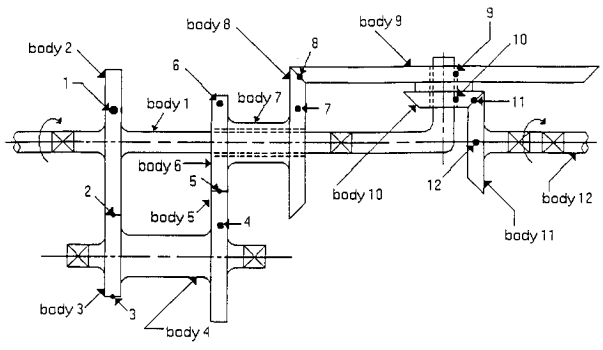

Fig. 2 Modeling of a transmission.

The holonomic and nonholonomic constraints at the velocity level can be written in compact form as

$$\mathcal{J}\mathcal{Y} = G(t) \tag{7}$$

where $\mathcal{J}$ is the Jacobian constraint matrix of order $c \times n$, c being the number of constraints in the system and n the number of generalized coordinates.

Differentiating the aforementioned equation once more and combining it with Eq. (1) after the elimination of the undetermined multipliers, we get

$$\mathcal{L}\dot{\mathcal{Y}} = \mathcal{R} \tag{8}$$

where

$$\mathcal{L} = [\mathcal{C}^T \mathcal{M}] \tag{9}$$

and

$$\mathcal{R} = \left[\mathcal{C}^T[\mathcal{F} - \mathcal{P} - \mathcal{Q}]\right] \tag{10}$$

$\mathcal{C}$ in the equation just presented is the orthogonal complement to the Jacobian matrix $\mathcal{J}$ and is obtained by the pseudo-uptriangular decomposition method.[25] Subsequent numerical integration of the governing equations of motion (8) would yield the time history of the generalized speeds or coordinates.

Constraints in Geared Transmissions: Rigid Gears/Shafts

Geared transmissions can be considered a multibody system, interconnected with flexible and rigid bodies. Basically the bodies involved could be classified into two types: shafts and gears.

Gears are mounted on the shafts, which are parallel (spur gears) or at different angles (bevel and other types of gears). The constraints associated with the contact between the various bodies of a transmission can be categorized as contact between shafts and gears, and contact between gears and gears.

Figure 1a shows a four-body transmisison, with two shafts and two gears. Bodies 1 and 4 are the shafts, over which the gears with body numbers 2 and 3 are mounted. In this system, there are three contacting regions, indicated by 1, 2, and 3. Points 1 and 3 are the points where the gears are fixed to the shafts, whereas point 2 represents the contact between the teeth of the gears.

Three constraints could be applied at these three points, which reduces the four-degrees-of-freedom system to a single-degree-of-freedom system (if we assume one degree of freedom for each body). These constraints can be classified as type 1 or type 2.

A type 1 constraint is that between the shaft and gear, as shown by points 1 and 3 in Fig. 1a, whereas the teeth contact as shown by point 2 represents the type 2 constraint. These three constraints can be represented in mathematical form as

$$\kappa_{\text{outer}}^{1}\bar{\Omega}^{1} = \kappa_{\text{inner}}^{2}\bar{\Omega}^{2} \tag{11}$$

$$\kappa_{\text{inner}}^{3}\bar{\Omega}^{3} = \kappa_{\text{outer}}^{4}\bar{\Omega}^{4} \tag{12}$$

and

$$\frac{\kappa_{\text{outer}}^{2}}{\kappa_{\text{outer}}^{3}} = -\frac{\dot{\theta}^{3}}{\dot{\theta}^{2}} \tag{13}$$

where κ^i is the radius of the gear i, and the subscripts inner and outer represent the inner and outer radii of the gears. Since

$$\kappa_{\text{outer}}^{1} = \kappa_{\text{inner}}^{1} \tag{14}$$

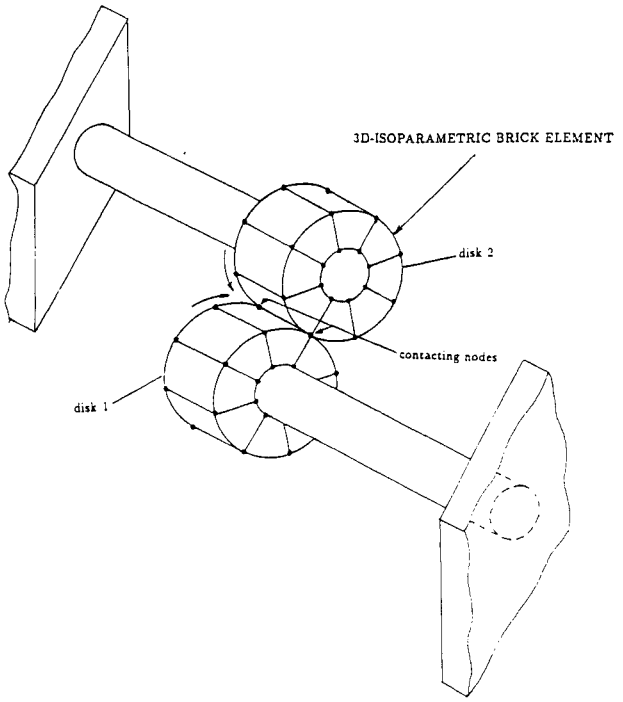

Fig. 3 System with two disks.

and

$$\kappa^3_{\text{inner}} = \kappa^4_{\text{outer}} \tag{15}$$

Eqs. (11) and (12) are reduced to the following form:

$$\bar{\Omega}^1 = \bar{\Omega}^2 \tag{16}$$

$$\bar{\Omega}^3 = \bar{\Omega}^4 \tag{17}$$

Writing the foregoing equations in matrix form, we get

$$[1 \quad -1]\begin{bmatrix}\dot{\theta}^1\\ \dot{\theta}^2\end{bmatrix} = 0 \tag{18}$$

$$[1 \quad -1]\begin{bmatrix}\dot{\theta}^3\\ \dot{\theta}^4\end{bmatrix} = 0 \tag{19}$$

and

$$\begin{bmatrix}\kappa^2_{\text{outer}} & \kappa^3_{\text{outer}}\end{bmatrix}\begin{bmatrix}\dot{\theta}^2\\ \dot{\theta}^3\end{bmatrix} = 0 \tag{20}$$

Note that the angular velocities Ω^1, Ω^2, Ω^3, and Ω^4 are simply represented by their generalized derivatives $\dot{\theta}$.

Combining the aforementioned three equations in matrix form, we obtain

$$\begin{bmatrix}1 & -1 & 0 & 0\\ 0 & \kappa^2_{\text{outer}} & \kappa^3_{\text{outer}} & 0\\ 0 & 0 & 1 & -1\end{bmatrix}\begin{bmatrix}\dot{\theta}^1\\ \dot{\theta}^2\\ \dot{\theta}^3\\ \dot{\theta}^4\end{bmatrix} = 0 \tag{21}$$

Comparing Eq. (21) with Eq. (7), we determine the Jacobian matrix

$$\mathcal{J} = \begin{bmatrix}1 & -1 & 0 & 0\\ 0 & \kappa^2_{\text{outer}} & \kappa^3_{\text{outer}} & 0\\ 0 & 0 & 1 & -1\end{bmatrix} \tag{22}$$

and

$$\mathcal{Y} = [\dot{\theta}^1 \quad \dot{\theta}^2 \quad \dot{\theta}^3 \quad \dot{\theta}^4]^T \tag{23}$$

In this case, $\dot{\Upsilon} = 0$ and $\dot{\eta} = 0$, since there are no translational velocities or flexibility effects.

One more important feature, which could be deduced from this discussion, is that the type 1 constraint results in Jacobian matrices of the form $[1 \quad -1]$, corresponding to the generalized coordinates associated with it [see Eq. (18) or (19)]. On the other hand, a type 2 constraint yields a Jacobian matrix of the form $[\kappa^2_{\text{outer}} \quad \kappa^3_{\text{outer}}]$, as shown by Eq. (20).

This feature can be used for automatically generating the Jacobian matrix $\mathcal{J}$ for the complete system if we know the type of constraints imposed at the different points. For example, if the point 1 in Fig. 1a has a type 1 constraint, then we insert a 1 and -1 in columns 1 and 2 of $\mathcal{J}$, corresponding to the generalized coordinates of the associated bodies, and the entries will have to occur in the first row, as they pertain to the first constraint of the system. Similar discussion holds for the second constraint, which is type 2, with the κ^2_{outer} and κ^3_{outer} being entered on the second row of $\mathcal{J}$ at columns 2 and 3, which correspond to bodies 2 and 3. Similarly, the procedure could be extended for defining the elements of position of the third constraint.

If we use the procedures just outlined, the Jacobian matrix for this system takes the following form:

$$\mathcal{J} = \begin{bmatrix}1 & -1 & 0 & 0 & 0 & 0 & 0\\ 0 & \kappa^2_{\text{outer}} & \kappa^3_{\text{outer}} & 0 & 0 & 0 & 0\\ 0 & 0 & 1 & -1 & 0 & 0 & 0\\ 0 & 0 & 0 & 1 & -1 & 0 & 0\\ 0 & 0 & 0 & 0 & \kappa^5_{\text{outer}} & 0 & \kappa^7_{\text{outer}}\\ 0 & 0 & 0 & 0 & 0 & 1 & -1\end{bmatrix} \tag{24}$$

Constraints with Flexible Bodies

The discussion in the previous section about rigid-body constraints can be easily extended for the case where the bodies are flexible (elastic).

Type 1 Constraint

Taking into consideration the effects of flexibility, we can modify Eq. (11) representing a type 1 constraint as

$$(\kappa^1_{\text{outer}} + \kappa^1_{\text{oflex}})(\bar{\Omega}^1 + \bar{\Omega}^1_{\text{flex}}) = (\kappa^2_{\text{inner}} + \kappa^2_{\text{iflex}})(\bar{\Omega}^2 + \bar{\Omega}^2_{\text{flex}}) \tag{25}$$

where κ^i_{oflex}, κ^i_{iflex}, and $\bar{\Omega}^i_{\text{flex}}$ represent the additional terms due to the effect of flexibility.

The foregoing constraint equation for contact point 1 in Fig. 1a can be expressed in terms of modal coordinates and written in compact matrix form as

$$\begin{bmatrix}\kappa^1_{\text{outer}} & \Lambda_{11} & \Lambda_{12} & -\kappa^2_{\text{inner}} & \Lambda_{21} & \Lambda_{22}\end{bmatrix}\begin{bmatrix}\dot{\theta}_1\\ \dot{\eta}_{11}\\ \dot{\eta}_{12}\\ \dot{\theta}_2\\ \dot{\eta}_{21}\\ \dot{\eta}_{22}\end{bmatrix} = 0 \tag{26}$$

where $\Lambda_{ij} = (\bar{\omega}_{ij} + \bar{\omega}^{\kappa}_{ij})$, $i = 1,2,\ldots,n$, and $j = 1,2,\ldots,m$, n and m being the number of bodies and of modal coordinates for each body, respectively. The $\bar{\omega}_{ij}$ and $\bar{\omega}^{\kappa}_{ij}$ are the coefficients associated with the derivatives of the modal coordinates $\dot{\eta}_{ij}$, which are picked up for the nodal-modal transformation matrix corresponding to the rotational and translational degrees of freedom.

Table 1 Shaft/gear configuration matrix

Shafts	1	4	7	1	1	12	Total
Gears	2	3	6	9	10	11	
		5	8				
No. of type 1 constraints	1	2	2	1	1	1	8

Table 2 Gear interaction matrix

Shafts	Pair 1	Pair 2	Total
1-4	2-3	—	
4-7	5-6	—	
7-1	8-9	—	
1-12	10-11	—	
No. of type 2 constraints	4	—	4

In a similar fashion, the constraint equation for the contacting point 3 in Fig. 1a can be written in simplified form, including the effects of flexibility as

$$\begin{bmatrix} \kappa^3_{\text{outer}} & \Lambda_{31} & \Lambda_{32} & -\kappa^4_{\text{inner}} & \Lambda_{41} & \Lambda_{42} \end{bmatrix} \begin{bmatrix} \dot{\theta}_3 \\ \dot{\eta}_{31} \\ \dot{\eta}_{32} \\ \dot{\theta}_4 \\ \dot{\eta}_{41} \\ \dot{\eta}_{42} \end{bmatrix} = 0 \tag{27}$$

The size of the Jacobian matrix $\mathcal{J}$ would now be of the order $c \times ng$, where ng is the number of generalized coordinates. In this case, additional entries from the nodal-modal transformation matrix corresponding to the modal coordinates for the bodies associated with the constraint under consideration are to be inserted at the required locations. These locations in $\mathcal{J}$ are governed by the constraint number (given by the row number) and generalized coordinate (given by the column number). They can be computed by the following equation:

$$t = (n-1)(m+1) + 1 \tag{28}$$

where n and m represent the total number of bodies in the system and the number of modal coordinates for each flexible body. A typical generalized speed vector $\bar{\Omega}$ with one rotational degree of freedom for each body, no translational degrees of freedom, and m modal coordinates can be expressed as

$$\bar{\Omega} = \left[\dot{\theta}_1, \dot{\eta}_{11}, \dot{\eta}_{12}, \ldots, \dot{\eta}_{1m}\dot{\theta}_2, \dot{\eta}_{21}, \dot{\eta}_{22}, \ldots, \dot{\eta}_{2m}\dot{\theta}_n, \dot{\eta}_{n1}, \dot{\eta}_{n2}, \ldots, \dot{\eta}_{nm}\right]^T \tag{29}$$

where $\dot{\theta}_i$, $i = 1,2,\ldots,n$ represent the rigid-body rotations and $\dot{\eta}_{ij}$, $i = 1,2,\ldots,n$, $j = 1,2,\ldots,m$ the modal coordinates associated with the flexible bodies.

Let us take a simple example of generating $\mathcal{J}$ for a system of 10 flexible bodies, having two modal coordinates for each one of them. Let there be a type 1 constraint between bodies 1 and 10. Let the number of such constraints be five. The size of the Jacobian matrix in this case will be 5×30. Substituting for body 1 in Eq. (28) the values $n = 1$ and $m = 2$, we get $t = 1$, which indicates that the first entry corresponding to the rigid-body rotation should be made in column 1, followed by two entries in the next two columns (i.e., 2 and 3) for the components of flexibility associated with the rotational and translational degrees of freedom, associated with the modal coordinates $\dot{\eta}_{ij} (i = 1,2,\ldots,n;\ j = 1,2,\ldots,m)$. These values correspond to those particular nodes that are under the constraint condition and are picked up from the nodal-modal transformation matrix. A similar discussion holds for the next set of entries for body number 10, except that the column numbers change to 28, 29, and 30 for the entries discussed here.

Having made the entries in the first row of $\mathcal{J}$ for the first constrained node, we will have to repeat the process five times for the five constraints under consideration. Thus, this process could be automated for any number of constraints and generalized coordinates.

The algorithm could be generalized for both rigid and flexible bodies by entering zeros for the $\bar{\omega}_{ij}$ $(i = 1,2,\ldots,n;\ j = 1,2,\ldots,m)$, as discussed earlier.

A sample $\mathcal{J}$ is shown:

$$\begin{bmatrix} \kappa^1_{\text{outer}} & \Lambda_{11} & \Lambda_{12} & 0 & 0 & 0 & -\kappa^3_{\text{inner}} & \Lambda_{31} & \Lambda_{32} \\ \kappa^1_{\text{outer}} & \Lambda_{11} & \Lambda_{12} & -\kappa^2_{\text{inner}} & \Lambda_{21} & \Lambda_{22} & 0 & 0 & 0 \\ 0 & 0 & 0 & \kappa^2_{\text{outer}} & \Lambda_{21} & \Lambda_{22} & -\kappa^3_{\text{inner}} & \Lambda_{31} & \Lambda_{32} \end{bmatrix} \tag{30}$$

Type 2 Constraint

The velocity of the common point of contact q between the two bodies i and j with the type 2 constraint can be written using a general relationship as

$$V^i_q = V^{ij} V^j_q \tag{31}$$

where V^i_q and V^j_q represent, respectively, the velocity of contact point q on bodies i and j, V^{ij} is the relationship between V^i_q and V^j_q that can be expressed in terms of i_x and i_y, the transmission ratios in the x and y directions (see Ref. 18 for more details) being

$$V^{ij} = \begin{bmatrix} i_x & 0 & 0 \\ 0 & i_y & 0 \\ 0 & 0 & 1 \end{bmatrix} \tag{32}$$

Thus, the constraint equation for the type 2 constraint can be written from Eq. (31) as

$$V^i_q - V^{ij} V^j_q = 0 \tag{33}$$

Using the concepts of partial velocity matrices and the equations for the velocity of an arbitrary point, we can write the velocities V^i_q and V^j_q as

$$V^i_q = \gamma^i_q \Omega + \nu^i \Upsilon + \beta^i_q \dot{\eta} \tag{34}$$

and

$$V^j_q = \gamma^j_q \Omega + \nu^j \Upsilon + \beta^j_q \dot{\eta} \tag{35}$$

where γ, ν, and β are, respectively, the partial velocity matrices associated with the rigid-body rotational velocity (Ω), rigid-body translational velocity (Υ), and the derivative of the modal coordinates ($\dot{\eta}$).

Substituting the expression for V^i_q and V^j_q in Eq. (33), we get

$$\gamma^i_q \Omega + \nu^i \Upsilon + \nu^i_q \dot{\eta} - V^{ij}\left[\gamma^j_q \Omega + \nu^j \Upsilon + \beta^j_q \dot{\eta}\right] = 0 \tag{36}$$

Simplifying further, we can write the foregoing equation as

$$\begin{bmatrix} (\gamma^i_q - V^{ij}\gamma^j_q) & (\nu^i_q - V^{ij}\nu^j_q) & (\beta^i_q - V^{ij}\beta^j_q) \end{bmatrix} \begin{bmatrix} \Omega \\ \Upsilon \\ \dot{\eta} \end{bmatrix} = 0 \tag{37}$$

This constraint equation can be written in the context of point 2 in Fig. 1a as follows:

$$\begin{bmatrix} (\gamma^2_2 - \gamma^3_2) & (\beta^2_2 - \beta^3_2) \end{bmatrix} \begin{bmatrix} \Omega \\ \dot{\eta} \end{bmatrix} = 0 \tag{38}$$

where $\Upsilon = 0$.

Table 3 Identification of the system constraints

Constraint no.	Body 1	Body 2	Constraint type
1	1	2	1
2	4	3	1
3	4	5	1
4	7	6	1
5	7	8	1
6	1	9	1
7	1	10	1
8	12	11	1
9	2	3	2
10	5	6	2
11	8	9	2
12	10	11	2

The aforementioned case is a simple one with one pair of contacting points. This could be extended to more general cases where the contact is assumed between surfaces having more pairs of contacting points. The node numbers for each pair of contacting points associated with a particular constraint number in column 1 of Table 3 will have to be specified. Based on this user-supplied information, the code can generate the required Jacobian matrix. The switching of the constraints could be achieved by changing the node numbers of the contacting nodes with time and using the right coefficient matrices in the constraint equations given here.

The foregoing discussion could be extended further for dealing with the contact problem between flexible meshing gear teeth as shown in Fig. 4. A detailed explanation of this can be found in Ref. 26. The governing equations of motion (8) will make use of the constraint equation (37) for type 2 constraints for all the pairs of contacting nodal points on the surface of the meshing gear teeth, which will be suitably updated in time. Thus, in this fashion, the dynamic analysis of a complete gear train/transmission could be carried out by extending the case to more than two flexible bodies.

Configuration/Interaction Matrices

As the number of bodies in the system increase, keeping track of the number/type of constraints and the bodies associated with them becomes a bit tedious. In order to make this task easy, we introduce a few tables based on the system configuration and interaction that might assist us in identifying the constraints, their types, and the bodies associated with them, thereby defining the assembly procedure for the constraint matrix $\mathcal{J}$.

In order to demonstrate the convenience and importance of the table discussed here and its subsequent computer implementation for automatic generation of Jacobian matrix $\mathcal{J}$, let us examine a more complicated system, as shown in Fig. 2.

The shaft-gear configuration Table 1 gives the total number of shafts and gears associated with a type 1 constraint. Table 2 gives the gear interaction matrix for type 2 constraints. Adding the entries for all the columns in Table 1 gives the total number of type 1 constraints, as shown in the last column. Thus, for the system under consideration, the total number of type 1 constraints is eight.

In a similar fashion, the total number of type 2 constraints is given by counting the entries of pairs in the columns, which is shown in the last row. There could be more than one pair of gears on a shaft. In the present example, there is no such occurrence. Thus, based on the information given in Tables 1 and 2, we can write the details of the constraints as follows.

Combining Tables 1 and 2, we generate Table 3 to assist us in the assembly of the global constraint Jacobian matrix $\mathcal{J}$ of the transmission system. The first column of Table 3 gives the total number of constraints. The second and third columns present the two bodies associated with the constraint in column 1. The last column offers the type of constraint.

V. Implementation on IBM 3090-600j

The foregoing algorithmic procedure is implemented on an IBM 3090-600j supercomputer. The code developed has long vectors/arrays. This feature makes it a potential candidate for pipe-lining in modern vector-processor-equipped supercomputers. This technique allows the overlapping of instructions to a sequence of operands as compared to a single operand in a scalar processor. Thus, speedup is achieved by a kind of microparallelism in which different stages of the pipeline work simultaneously on different data. In general, performance increases with the vector length up to a limit governed by the section size of the vector pipe. The section size refers to the number of elements a vector pipe could hold at a particular time. The section size varies with the machine, e.g., 256 in IBM 3090 and 64 in the CRAY.

An effort was made to improve the efficiency of execution of the implemented code by reducing the cpu time and vectorizing the code. This was carried out at both the compiler option level (outside the code) and the Do-loop level (inside the code) in the computationally intensive areas. In particular, the concepts of promoting the scalar variables to vectors on the left-hand side of the expressions were found to be more effective in certain computationally intensive areas.

Tables 4 and 5 give a comparison between the cpu time taken for compilation and execution of the code using optimization levels 1 and 2 with and without vectorization. These values are taken from the simulation presented in this paper. The cpu time was recorded at the compilation stage using optimization levels 2 and 3, with and without the vector options. The increase in computational efficiency was found to be on the order of 1.5 to 2.0. It is also important to note from the values shown that even though the computational efficiency increases with the vectorization process, the compilation time itself goes up by a significant amount.

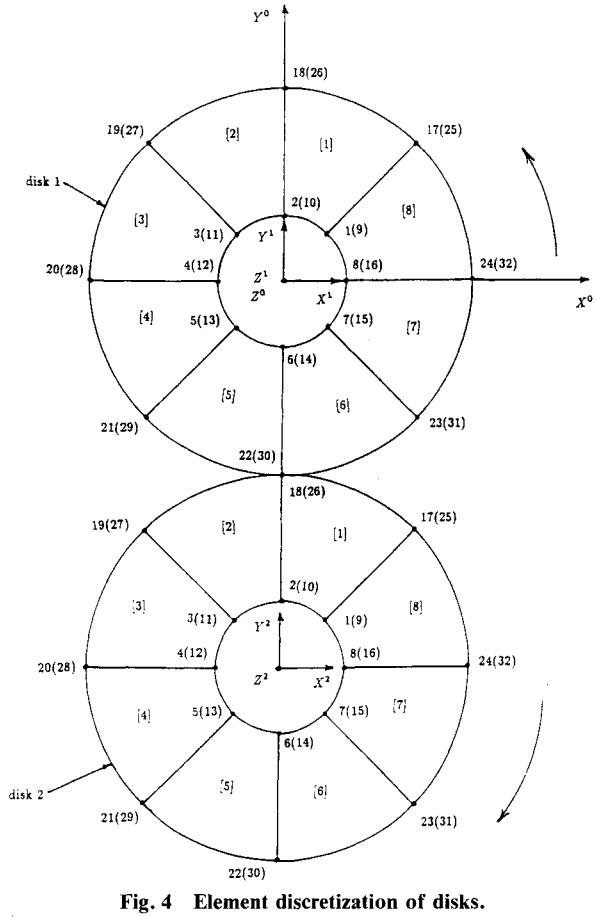

Fig. 4 Element discretization of disks.

Table 4 Comparison of cpu time (s) taken for compilation

Optimization 2: no vector	Optimization 3: no vector	Optimization 2: vector	Optimization 3: vector
13.15	15.73	68.66	67.75

Table 5 Comparison of cpu time (s) taken for execution

Optimization 2: no vector	Optimization 3: no vector	Optimization 2: vector	Optimization 3: vector
12.01	9.60	6.89	6.84

VI. Illustrative Example

A detailed discussion pertaining to the constraints at the contacting nodal points on the gear teeth is given in Sec. 4.2 of Ref. 26. Let us consider at this point a simplified case of two contacting disks. For the example at hand, we consider a more specialized case, in which the diameters of the disks are the same as those shown in Fig. 3. The nodal points located on the periphery of the disks assumed to be initial points of contact are shown in Fig. 3. The disks are discretized using the three-dimensional-isoparametric brick elements[20] with eight nodes. Each node has six degrees of freedom (three rotational and three translational). Each disk has eight elements with 32 nodes as shown in Fig. 4. Thus for the system of two disks, the total degrees of freedom are 384. The problem is simplified further by allowing only the translational degrees of freedom at each node along the X,Y directions and a rotation in the Z direction. The constraint equations are generated automatically using Eq. (37).

The disks are made to rotate in opposite directions with the type 2 constraints applied at the contacting nodal points at 1200 rpm (around 125 rad/s, which corresponds to the speed of the gearing system used in helicopter transmission). Based on this speed, the time in seconds Δt needed for a rotation of 45 deg is computed. Thus, by selecting the time interval Δt, the switching of constraints is carried out by specifying the nodal points that follow. It should be noted at this point that the time interval Δt will have to be adjusted due to the flexibility effect and the subsequent change in the following node's location. For simplicity the nodal contact points are selected a priori. Simulation is carried out by selecting first and second modes in the first case and eighth and ninth modes in the second case. The computation of the constraint forces associated with the generalized coordinates is completed and plotted for both cases. The constraint Jacobian matrices are updated based on the change in node numbers, which is specified. The eigenvalues corresponding to the first, second, eighth, and ninth modes were found to be 4.335×10^3, 4.822×10^3, 6.279×10^5, and 2.605×10^6, respectively. The eigenvalue corresponding to the lowest natural frequency of the system was determined to be 2.5×10^8. The mode numbers 64 and 65 were found to be the associated mode shapes with the closest eigenvalues, 9.973×10^7 and 4.129×10^8, respectively. These mode numbers were used for the simulation of the system, which was excited at the natural frequency of 15833.0 rad/s. The effect of this excitation at the selected modes associated with the generalized coordinates was also plotted.

The reason for discussing the effects of constraint forces and how they vary in time is simply to highlight how the method presented in this paper could be used in predicting contact forces in gears. Figure 5 shows the variation of constraint forces corresponding to the generalized coordinates θ_1 and θ_2 (rigid-body rotation), for both disks, corresponding to the first and second modes. We can see that these forces have an oscillatory effect due to the vibration of the bodies, though the magnitudes are small. The variation in these plotted constraint forces occurs during the time period in which the disks have rotated through one complete revolution. It is interesting to note that the reacting constraint torques at the center of the disks have the same sign for both bodies. The change in magnitude as shown by the dotted lines in Fig. 5 is due to the effect of flexibility and vibrations associated with the bodies. Figure 6 shows the effect of exciting the system at 15833.0 rad/s by selecting the proper mode numbers (64 and 65) as discussed earlier. The constraint forces as expected in this case are extremely high, by an order of 10^4 to 10^5. This is due mainly to the resonance effects as the disks are rotating at a frequency close to their natural frequencies. The corresponding constraint forces associated with the rigid-body rotations θ_1 and θ_2 are plotted in Fig. 6 and shown by the discontinuous solid lines. These are superimposed on the constraint forces plotted in Fig. 5 for the case of first and second modes, where the system was rotated at a speed of 1200 rpm (125 rad/s). Figure 7 gives the plot for the variation of constraint forces associated with the rigid-body rotations, when eighth and ninth

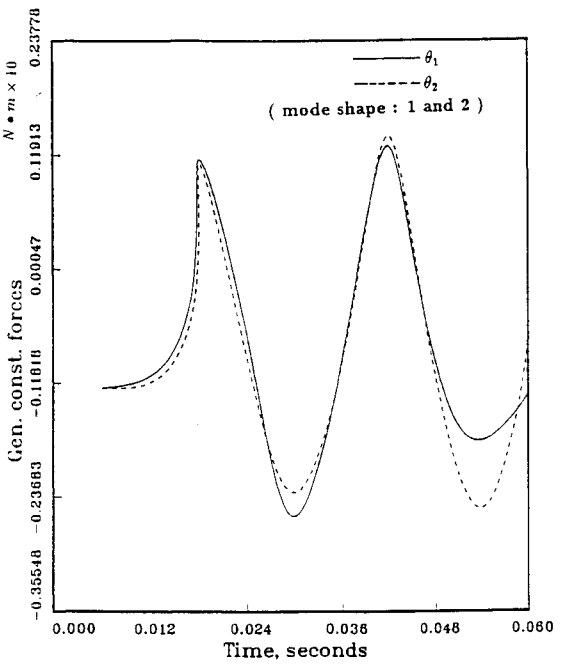

Fig. 5 Generalized constraint forces (1).

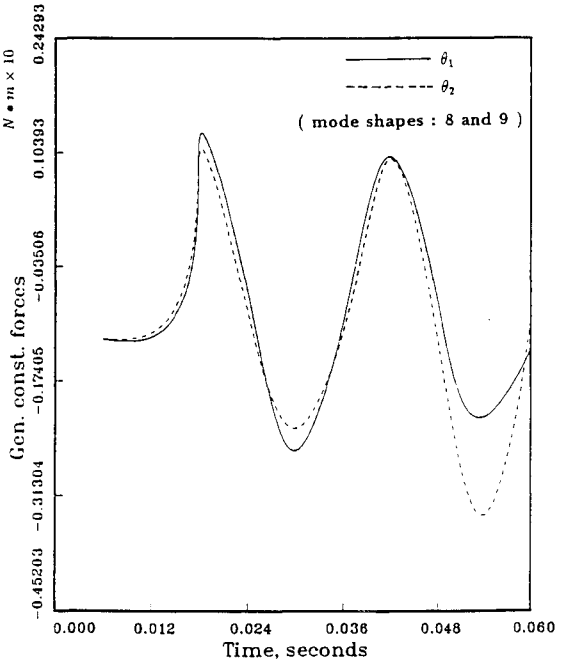

Fig. 6 Generalized constraint forces (2).

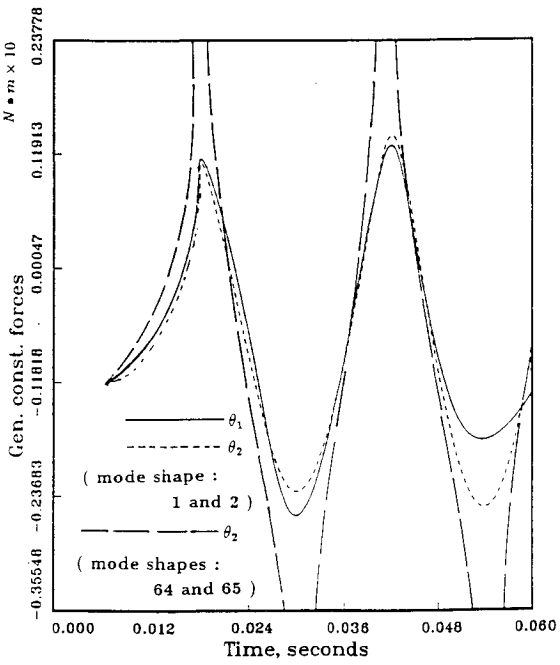

Fig. 7 Generalized constraint forces (3).

modes were selected, at a rotational speed of 1200 rpm. It can be seen from the plot that the variation of constraint forces is similar to the case in which the first and second modes were selected, though the magnitudes are slightly changed.

VII. Conclusions

In this paper a comprehensive algorithmic procedure has been developed for handling the constraints in flexible rotorcraft/transmission systems. The process of automatic generation of constraint Jacobian matrices is explained through configuration and interaction matrices with various examples. These matrices help in identifying the number/type of constraints and the bodies associated with them in the system. The implementation of the algorithm on an IBM 3090-600j has been carried out in such a way as to exploit the vector processing capabilities of the machine. Much is gained from the large vector content of the algorithm by suitable vectorization at the Do-loop level (inside the code) and complier level (outside the code). The intent of this paper is to extend the dynamics of flexible multibody systems to handle problems of different types such as rotorcraft systems that require a different procedure in evaluating for the time constraint conditions describing the bodies in contact. An illustrative example has been presented. The time histories of the generalized contact forces are presented and the effect on the constraint forces due to the excitation at frequencies close to the natural frequency is also studied.

Acknowledgments

The support of this work by NASA/LEWIS NAG3-1092 is gratefully acknowledged. The authors wish to thank Mark Valco for his keen interest and encouragement during the course of this work. We would also like to thank the Cornell National Supercomputing Facility for the use of its computer.

References

[1]Gunter, E. J., "Dynamic Stability of Rotor-Bending Systems," *NASASP,* Vol. 113, No. 29, 1966.

[2]Rankine, W. A., "On the Centrifugal Force of Rotating Shafts," *Engineer,* London, 1985.

[3]Vance, J. M., and Royal, A. C., "High Speed Rotor Dynamics: An Assessment of Current Technology for Small Turboshaft Engines," *Journal of Aircraft,* Vol. 12, No. 4, 1975, pp. 295-305.

[4]Gunter, E. J., and Barrett, L. E., "Dynamic Characteristics of a Two-Spool Gas Turbine Helicopter Engine," *Proceedings of the Conference on Stability and Dynamic Response of Rotors with Squeeze Film Bearings* (Charlottesville, VA), May 8-10, 1979.

[5]Chivens, D. R., and Nelson, H. D., "The Natural Frequencies and Critical Speeds of a Rotating Flexible Shaft-Disk System," *Journal of Engineering for Industry* (Paper 74-WA/DE-14), 1974.

[6]Ehrich, F. F., "Identification and Avoidance of Instabilties and Self-Excited Vibrations in Rotating Machinery," ASME Paper 72-DE-21, 1972.

[7]Sachadeva, T. D., and Ramakrishnan, V., "A Finite Element Solution for the Two-Dimensional Elastic Contact Problems," *International Journal of Numerical Methods in Engineering,* Vol. 17, No. 8, 1981, pp. 1257-1271.

[8]Francavilla, A., and Zienkiewicz, O. C., "A Note on Numerical Computation of Elastic Contact Problems," *International Journal of Numerical Methods in Engineering,* Vol. 2, No. 1, 1970, pp. 5-32.

[9]Tseng, J., and Olson, M. D., "The Mixed Finite Element Method Applied to Two-Dimensional Elastic Contact Problem," *International Journal of Numerical Methods in Engineering,* Vol. 17, No. 7, 1981, pp. 991-1014.

[10]Oden, J. T., and Pires, E. B., "Numerical Analysis of Certain Contact Problems in Elasticity with Non-Classical Friction Laws," *Computers and Structures,* Vol. 16, No. 1-4, 1983, pp. 481-485.

[11]Schafer, H., "A Contribution to the Solution of a Contact Problem with the Aid of Bond Elements," *Computer Method, Applied Mechanics and Engineering,* Vol. 6, No. 3, 1975, pp. 335-354.

[12]Chan, S. K., and Tuba, I. S., "A Finite Element Method for Contact Problems of Solid Bodies—Part I. Theory and Validation," *International Journal of Mechanical Science,* Vol. 13, No. 7, 1971, pp. 615-625.

[13]Bathe, K. J., and Chaudhary, A., "A Solution Method for Planar and Axisymmetric Contact Problems," *International Journal of Numerical Methods in Engineering,* Vol. 21, No. 1, 1985, pp. 65-88.

[14]Vijayakar, S. M., Busby, R. H., and Houser, D. R., "Finite Element Analysis of Quasiprismatic Bodies Using Chebyshev Polynomials," *International Journal of Numerical Methods in Engineering,* Vol. 24, No. 8, 1987, pp. 1461-1477.

[15]Chandrashekaran, N., Haisler, W. E., and Goforth, R. E., "A Finite Element Solution Method for Contact Problems with Friction," *International Journal of Numerical Methods in Engineering,* Vol. 24, No. 3, 1987, pp. 477-495.

[16]Simo, J. C., Wriggers, P., Schweizerhof, K. H., and Raylor, R. L., "Finite Deformation Post-Buckling Analysis Involving Inelasticity and Contact Constraints," *International Journal of Numerical Methods in Engineering,* Vol. 23, No. 5, 1986, pp. 779-800.

[17]Talaslidis, D., and Panagiotopoulos, P. D., "A Linear Finite Element Approach to the Solution of the Variational Inequalities Arising in Contact Problems of Structural Dynamics," *International Journal of Numerical Methods in Engineering,* Vol. 18, No. 10, 1982, pp. 1505-1520.

[18]Fredriksson, B., "Finite Element Solution of Surface Non-Linearities in Structural Mechanics with Special Emphasis to Contact and Fracture Mechanics Problems," *Computers and Structures,* Vol. 6, No. 4/5, 1976, pp. 281-290.

[19]Ider, S. K., and Amirouche, F. M. L., "Non-Linear Modeling of Multibody System Dynamics Subjected to Variable Constraints," *Journal of Applied Mechanics,* Vol. 56, No. 2, 1989, pp. 444-447.

[20]Amirouche, F. M. L., and Shareef, N. H., "Implementation of 3D-Isoparametric Finite Elements on Supercomputer for the Formulation of Recursive Dynamical Equations of Multibody Systems," *Non-Linear Dynamics,* Vol. 2, No. 5, 1991, pp. 319-334.

[21]Amirouche, F. M. L., and Shareef, N. H., "Gain in Computational Efficiency by Vectorization in the Dynamic Simulation of Multi-Body Systems," *Computers and Structures,* Vol. 41, No. 2, 1991, pp. 293-302.

[22]Gibson, D. H., Rain, D. W., and Walsh, H. F., "Engineering and Scientific Processing on the IBM 3090," *Systems Journal,* Vol. 25, No. 1, 1986.

[23]Levesque, J. M., and Williamson, J. W., *A Guidebook to Fortran on Supercomputers,* Academic, New York, 1989.

[24]Metcalf, M., *Fortran Optimization,* Academic, New York, 1985.

[25]Amirouche, F. M. L., and Tongyi, J. "Automatic Elimination of Undetermined Multipliers in Kane's Equations Using a Pseudo-Uptriangular Decomposition Method," *Computers and Structures,* Vol. 27, No. 2, 1987, pp. 203-210.

[26]Amirouche, F. M. L., Shareef, N. H., and Xie, M., "Dynamic Analysis of Flexible Gear Trains/Transmissions—An Automated Approach," *Journal of Applied Mechanics,* Vol. 59, No. 4, 1992.